J Mater Sci (2013) 48:5930–5937
DOI 10.1007/s10853-013-7388-4

Fabrication and luminescence properties of $YF_3:Eu^{3+}$ hollow nanofibers via coaxial electrospinning combined with fluorination technique

Dan Li · Jinxian Wang · Xiangting Dong · Wensheng Yu · Guixia Liu

Received: 19 January 2013 / Accepted: 14 April 2013 / Published online: 24 April 2013

Abstract Polyvinyl pyrrolidone (PVP)–PVP/[$Y(NO_3)_3$ + $Eu(NO_3)_3$] core–sheath composite nanofibers were prepared by coaxial electrospinning, and then $Y_2O_3:Eu^{3+}$ hollow nanofibers were synthesized by calcination of the as-prepared composite nanofibers. For the first time, $YF_3:Eu^{3+}$ hollow nanofibers were successfully fabricated by fluorination of the $Y_2O_3:Eu^{3+}$ hollow nanofibers via a double-crucible method using NH_4HF_2 as fluorinating agent. The morphology and properties of the products were investigated in detail by X-ray diffraction, scanning electron microscope (SEM), transmission electron microscope (TEM), and fluorescence spectrometer. $YF_3:Eu^{3+}$ hollow nanofibers were pure orthorhombic phase with space group Pnma and were hollow-centered structure with the mean diameter of 211 ± 29 nm. Fluorescence emission peaks of Eu^{3+} in the $YF_3:Eu^{3+}$ hollow nanofibers were observed and assigned to the energy levels transitions of $^5D_0 \rightarrow {}^7F_1$ (587 and 593 nm), $^5D_0 \rightarrow {}^7F_2$ (615 and 620 nm), and the $^5D_0 \rightarrow {}^7F_1$ hypersensitive transition at 593 nm was the dominant emission peak. Moreover, the emitting colors of $YF_3:Eu^{3+}$ hollow nanofibers were located in the red region in CIE chromaticity coordinates diagram. The luminescent intensity of $YF_3:Eu^{3+}$ hollow nanofibers was increased remarkably with the increasing doping concentration of Eu^{3+} ions and reached a maximum at 7 mol% of Eu^{3+}. This preparation technique could be applied to prepare other rare earth fluoride hollow nanofibers.

D. Li · J. Wang · X. Dong (✉) · W. Yu · G. Liu
Key Laboratory of Applied Chemistry and Nanotechnology at Universities of Jilin Province, Changchun University of Science and Technology, Changchun 130022, China
e-mail: dongxiangting888@163.com

Introduction

In the past few years, nanosized materials have been a subject of extensive research due to their unique properties. The rare earth fluoride luminescent nanomaterials have recently attracted much attention owing to their peculiar physical and chemical properties, for example, low phonon energy, high ionicity, high resistivity, and high anionic conductivity [1]. YF_3 is one of the most important host crystals for lanthanide-doped phosphors, providing a wide band gap (>10 eV) and suitable Y^{3+} sites where Y^{3+} can be easily substituted by other trivalent rare earth ions without additional charge compensation [2]. $YF_3:Ln^{3+}$ nanomaterials have wide and potential applications in optical devices, phosphors, down/up conversion luminescent materials [1, 3], etc.

By far, a variety of efforts have been devoted to developing several simple and efficient methods for the fabrication of YF_3 or $YF_3:Ln^{3+}$ luminescent nanomaterials with different morphologies and sizes, such as nanocrystals, nanowires, nanorods, nanobundles, nanoflowers, nanoplates, etc. [4–12]. Typical synthetic methods include hydrothermal methods [4, 5, 13], coprecipitation [14], microemulsion [6–8], pyrolysis [15, 16], solid state reaction [17], ultrasonic-assisted route [9, 18], microwave synthesis [2, 10], solvent extraction route [19], liquid–solid–solution (LSS) phase transfer synthesis [20], etc. Nevertheless, no reports on the preparation of $YF_3:Ln^{3+}$ hollow nanofibers are found in the literature. Hollow nanofibers double the surface area compared with common solid nanofibers, which is very useful in surface-related applications such as chemical sensors or photocatalysis [21].

Electrospinning is a simple, straightforward and versatile method to fabricate micro- and nanofibers of various

materials, including rare earth oxyfluoride nanofibers [22], rare earth oxide nanofibers [23–25] and hollow nanofibers [26], core–shell structured coaxial nanofibers [27] and nanobelts [28, 29], etc. The electrospinning-based synthesis method of hollow nanofibers, which includes monoaxial [30, 31] and coaxial electrospinning [21] method, has also been reported. The key point of coaxial electrospinning is the dual nozzle spinneret which has a smaller (inner) capillary inside the bigger (outer) capillary at the coaxial position [32].

Recently, Yang et al. [22] prepared the pure phase YOF:Ln^{3+} nanofibers via sintering the electrospun $RE(CF_3COO)_3$/PVP composite fibers at high-temperature. Nevertheless, pure phase YF_3:Ln^{3+} cannot be easily prepared using this process, because YF_3 is easy to be oxidized at high calcination temperature. Hence, preparation of pure phase YF_3:Ln^{3+} hollow nanofibers remains an important and challenging subject of study. In this paper, Y_2O_3:*x*%Eu^{3+} hollow nanofibers were prepared through calcining the coaxial electrospun PVP@PVP/[$Y(NO_3)_3$ + $Eu(NO_3)_3$] core–sheath composite nanofibers at 700 °C. YF_3:*x*%Eu^{3+}[x = 1,3,5,7,9, x stands for molar ratio of Eu^{3+} to (Eu^{3+}+Y^{3+})] hollow nanofibers were fabricated by fluorination of Y_2O_3:*x*%Eu^{3+} hollow nanofibers via a double-crucible method we newly proposed for the first time. The samples were systematically characterized and some meaningful results were obtained.

Experimental sections

Chemicals

Polyvinyl pyrrolidone (PVP) (K90, Mr = 1300000, AR) was bought from Tiantai Chemical Co., Ltd. Yttrium oxide (Y_2O_3) (99.99 %) and europium oxide (Eu_2O_3) (99.99 %) were purchased from Kemiou Chemical Co., Ltd. *N*,*N*-dimethylformamide (DMF, AR) and ammonium hydrogen fluoride (NH_4HF_2, AR) were purchased from Sinopharm Chemical Reagent Co., Ltd. Nitric acid (HNO_3, AR) and absolute ethyl alcohol were bought from Beijing Chemical Factory. All chemicals were directly used as received without further purification.

Preparation of PVP@PVP/[$Y(NO_3)_3$ + $Eu(NO_3)_3$] core–sheath composite nanofibers via coaxial electrospinning

In the preparation of sheath precursor solution, 1.8 g of $RE(NO_3)_3{\cdot}6H_2O$ (RE = Y^{3+} and Eu^{3+}) dissolved in 16.4 g of DMF, and then 1.8 g of PVP was added into the above solution under magnetic stirring for 4 h to form 20 g of homogeneous transparent sheath solution. In the sheath solution, the mass ratios of PVP, rare earth nitrates and DMF were equal to 9:9:82. To prepare the core precursor solution, 1.35 g of PVP was dissolved in 13.65 g of absolute ethyl alcohol under magnetic stirring for 4 h to form 15 g of homogeneous transparent core solution.

Subsequently, a homemade coaxial electrospinneret was used in this study. A coaxial nozzle was designed to make core–sheath composite nanofibers, as shown in Fig. 1, the core solution was injected into the inner plastic syringe while the sheath solution was loaded into the outer one. A flat iron net used as a fiber collector was put 16 cm away from the spinneret. The two solutions were electrospun at room temperature under a positive high voltage of 13 kV and relative humidity was 30–60 %, and PVP@PVP/[$Y(NO_3)_3$ + $Eu(NO_3)_3$] core–sheath composite nanofibers were acquired on the collector.

Fabrication of Y_2O_3:Eu^{3+} hollow nanofibers

The above PVP@PVP/[$Y(NO_3)_3$ + $Eu(NO_3)_3$] core–sheath composite nanofibers were calcined at 700 °C for 8 h with a heating rate of 1 °C/min. Then, the calcination temperature was decreased to 200 °C at a rate of 1 °C/min. Finally, samples were naturally cooled down to room temperature and Y_2O_3:Eu^{3+} hollow nanofibers were obtained.

Fabrication of YF_3:Eu^{3+} hollow nanofibers

Y_2O_3:Eu^{3+} hollow nanofibers were loaded into a small crucible. A few carbon rods were put into a big crucible, and then the small crucible was placed into the big crucible. Next, some NH_4HF_2 powders were loaded into the space between the two crucibles, and then the big crucible was covered with its lid. We call this process a double-crucible method. Finally, the crucibles were annealed at 280 °C for 2 h, then heated to 450 °C and remained for 3 h with the heating rate of 2 °C/min, then, the temperature was decreased to 200 °C at a rate of 1 °C/min followed by natural cooling down to ambient temperature. Thus, YF_3:Eu^{3+} hollow nanofibers were acquired.

Characterization methods

The as-prepared YF_3:Eu^{3+} hollow nanofibers were identified by a Rigaku D/max-RA X-ray powder diffractometer (XRD) with Cu Kα radiation. The operation voltage and current were kept at 30 kV and 20 mA, respectively. The morphology and internal structure of YF_3:Eu^{3+} hollow nanofibers were observed by a field emission scanning electron microscope (FESEM, XL-30, FEI Company) and a transmission electron microscope (TEM, JEM-2010). The excitation and emission spectra of samples were recorded

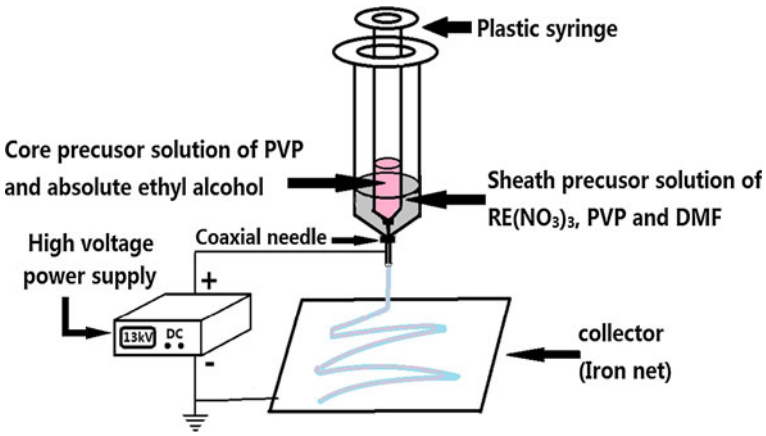

Fig. 1 Schematic diagram of the coaxial electrospinning spinneret and the electrospinning setup

with a HITACHI F-7000 fluorescence spectrophotometer using a Xe lamp as the excitation source. The histograms of diameters were drawn by Image-Pro Plus 6.0 and origin 8.5 softwares.

Results and discussion

Characterizations of the structure and morphology

Figure 2a shows the XRD patterns of Y_2O_3:Eu^{3+} hollow nanofibers (a) and YF_3:Eu^{3+} hollow nanofibers (b). It can be seen that XRD pattern of the Y_2O_3:Eu^{3+} hollow nanofibers is conformed to the cubic structure of Y_2O_3 (PDF#86-1107), and the space group is $Ia\bar{3}$. No peaks of any other phases or impurities are detected, indicating crystalline Y_2O_3:Eu^{3+} were obtained. The lattice constants of Y_2O_3:Eu^{3+} crystals are $a = b = c = 10.6102$ Å, respectively. The XRD analysis result of YF_3:Eu^{3+} hollow nanofibers demonstrates that the characteristic diffraction peaks [$2\theta = 24.6°$(101), 25.9° (020), 27.8°(111), 30.96°(210), 44.6°(221), 45.6°(112), 46.9°(131), 49.0°(230), 55.0°(321), 76.8°(223), etc.] of the sample can be easily indexed to those of the pure orthorhombic phase with primitive structure of YF_3 (PDF#70-1935), and the space group is Pnma. No characteristic peaks were observed for other impurities, the lattice constants of YF_3:Eu^{3+} crystals are $a = 6.354$ Å, $b = 6.854$ Å, $c = 4.395$ Å, respectively.

Figure 2b manifests XRD patterns of the YF_3:x%Eu^{3+} ($x = 1,3,5,7,9$) hollow nanofibers. As seen from the Fig. 2b, the XRD patterns of all samples are consistent with the orthorhombic structure of YF_3 (PDF#70-1935), and the space group is Pnma. In addition, with the increase of Eu^{3+} concentration, no obvious shifting of peaks can be detected, indicating that Y^{3+} may be substituted by Eu^{3+} successfully to form the luminescence center because of the similar radius between Y^{3+} and Eu^{3+}.

Figure 3a, b demonstrate FESEM images of Y_2O_3:Eu^{3+} hollow nanofibers and YF_3:Eu^{3+} hollow nanofibers. It can be clearly seen that the morphology and diameters of YF_3:Eu^{3+} hollow nanofibers are similar to those of Y_2O_3:Eu^{3+} hollow nanofibers and morphology of fibers is hollow-centered structure. Therefore, we can safely conclude that the fluorination technique, we proposed here, can retain the morphology of the precursor nanofibers. Histograms of diameters of these fibers are indicated in Fig. 4. The average diameters of Y_2O_3:Eu^{3+} hollow nanofibers and YF_3:Eu^{3+} hollow nanofibers are, respectively, 213 ± 42 and 211 ± 29 nm under the confidence level of 95 %.

The TEM images of Y_2O_3:Eu^{3+} hollow nanofibers and YF_3:Eu^{3+} hollow nanofibers are presented in Fig. 5. It is found that Y_2O_3:Eu^{3+} hollow nanofibers and YF_3:Eu^{3+} hollow nanofibers are composed of nanoparticles, and the diameters of Y_2O_3:Eu^{3+} and YF_3:Eu^{3+} hollow nanofibers are ca. 200 nm. The results are consistent with the results of SEM analysis. In the inset of Fig. 5b, the corresponding selected area electron diffraction (SAED) patterns of YF_3:Eu^{3+} hollow nanofibers exhibit typical polycrystalline diffraction patterns, indicating that polycrystalline YF_3:Eu^{3+} was obtained.

Energy dispersive spectrum (EDS) analysis

The EDS analysis shown in Fig. 6 manifests that the presence of Y, O, Eu corresponds to Y_2O_3:Eu^{3+}, and the presence of Y, F, Eu corresponds to YF_3:Eu^{3+}. C exists in YF_3:Eu^{3+} hollow nanofibers due to carbon rods loaded into the big crucible during the fluorination process. Si comes from Si carrier for bearing the sample and Au peak is from the conductive film of Au-plated on the sample for SEM observation.

Photoluminescence properties

Figure 7 demonstrates the PL excitation (monitored by 593 nm) and emission (excited by 394 nm) spectra of the YF_3:7%Eu^{3+} hollow nanofibers. The excitation spectrum

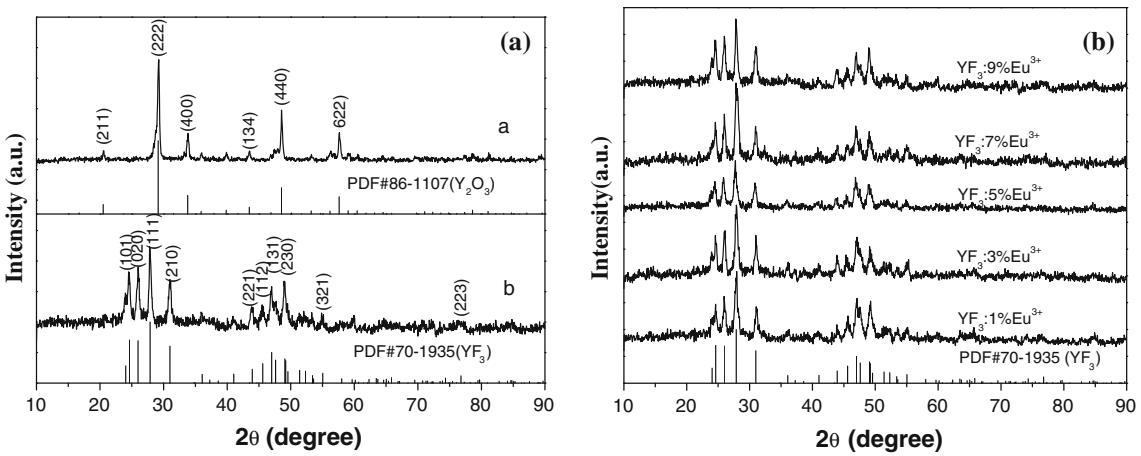

Fig. 2 XRD patterns of Y_2O_3:Eu^{3+} (*a*) and YF_3:Eu^{3+} (*b*) *hollow* nanofibers (**a**), and YF_3:*x*%Eu^{3+} (*x* = 1,3,5,7,9) *hollow* nanofibers (**b**)

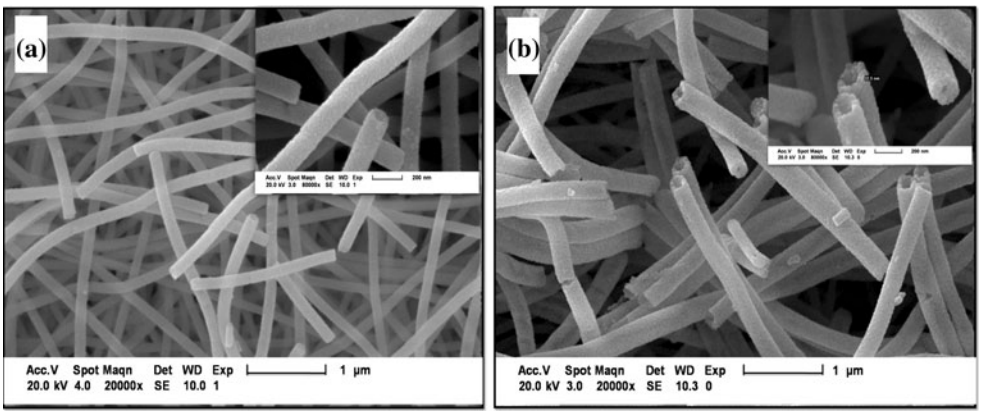

Fig. 3 FESEM images of Y_2O_3:Eu^{3+} *hollow* nanofibers (**a**) and YF_3:Eu^{3+} *hollow* nanofibers (**b**)

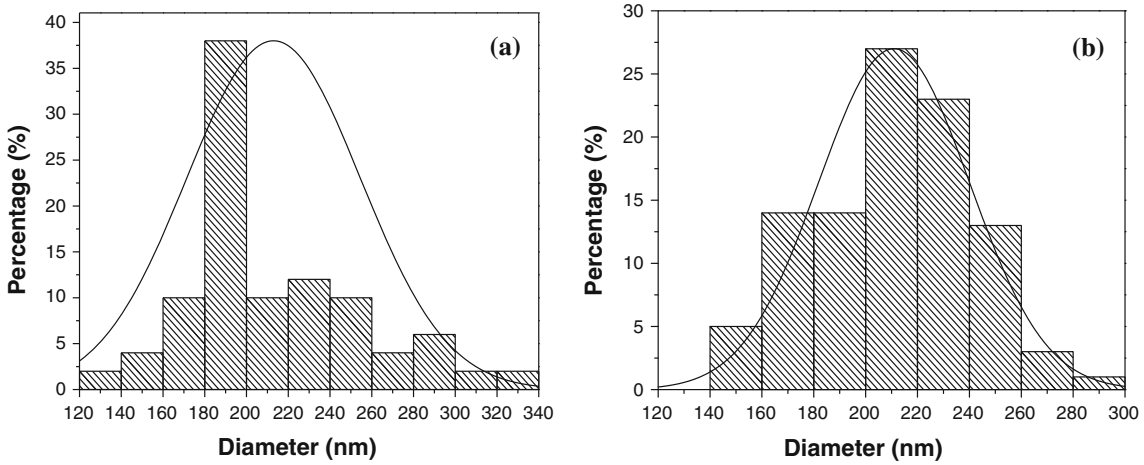

Fig. 4 Histograms of diameters of Y_2O_3:Eu^{3+} *hollow* nanofibers (**a**) and YF_3:Eu^{3+} *hollow* nanofibers (**b**)

(Fig. 7a) is dominated by the $^7F_0 \rightarrow {}^5L_6$ transition of Eu^{3+} ions centered at about 394 nm. The position of other peaks is practically identical to the characteristic absorption bands for f–f transitions in Eu^{3+} ions [33]. The emission spectrum (Fig. 7b) consists of seven main peaks at 555, 587, 593, 615, 620, 651, and 692 nm, which originate from the $^5D_1 \rightarrow {}^7F_2$, $^5D_0 \rightarrow {}^7F_1$, $^5D_0 \rightarrow {}^7F_2$, $^5D_0 \rightarrow {}^7F_2$, $^5D_0 \rightarrow {}^7F_3$, and $^5D_0 \rightarrow {}^7F_4$ transitions of Eu^{3+}

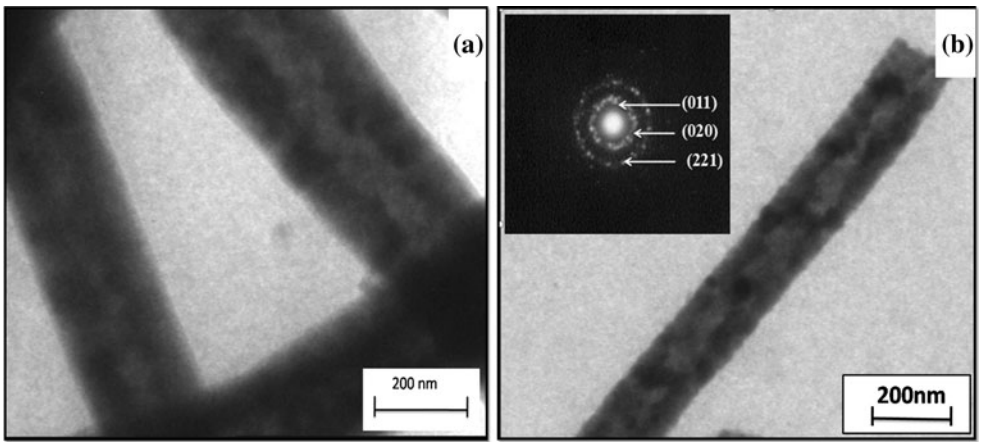

Fig. 5 TEM images of Y_2O_3:Eu^{3+} *hollow* nanofibers (**a**) and YF_3:Eu^{3+} *hollow* nanofibers (**b**), the *inset* shows the SAED patterns of YF_3:Eu^{3+} *hollow* nanofibers

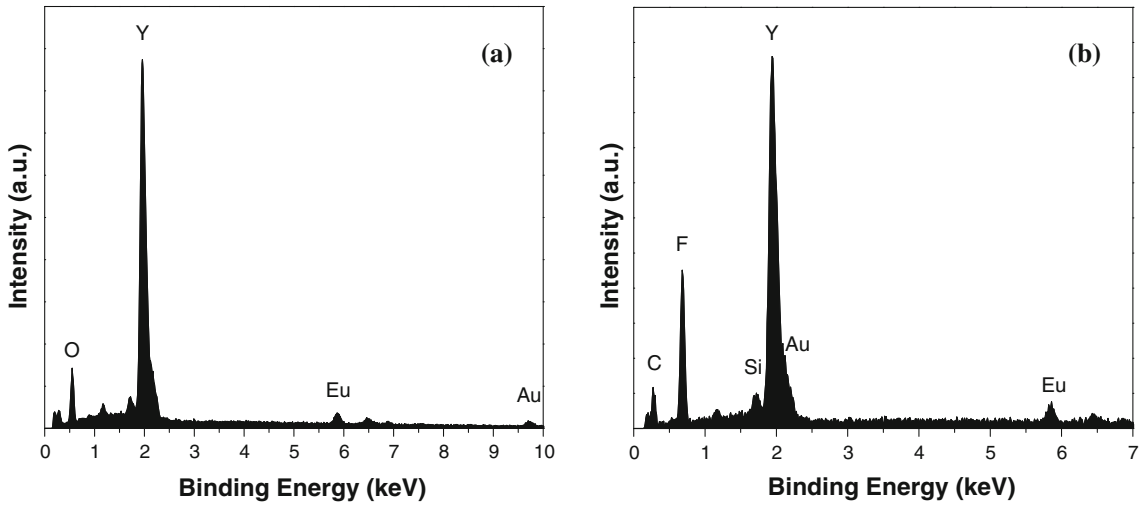

Fig. 6 EDS spectra of Y_2O_3:Eu^{3+} *hollow* nanofibers (**a**) and YF_3:Eu^{3+} *hollow* nanofibers (**b**)

ions, respectively. Among these emission peaks, the red emission at 593 nm attributed to $^5D_0 \rightarrow {}^7F_1$ transition of Eu^{3+} ions is the strongest one.

Figure 8 shows the excitation spectra and emission spectra of YF_3:Eu^{3+} hollow nanofibers with different doping concentrations of Eu^{3+} ions. It is found that the peak positions and spectral shapes of excitation and emission spectra do not vary with Eu^{3+} concentration for YF_3:Eu^{3+} hollow nanofibers, but the intensity of excitation and emission peaks for YF_3:x%Eu^{3+} hollow nanofibers strongly depends on the doping concentration of Eu^{3+} ions and the strongest excitation and emission spectra can be obtained when the doping molar concentration of Eu^{3+} is 7 %. Obviously, the luminescence intensity of YF_3:Eu^{3+} hollow nanofibers increases with the increase of the concentration of Eu^{3+} from the beginning, reaching a maximum value with the Eu^{3+} concentration of 7 %, and then decrease with the further increase in Eu^{3+} concentration. Below this value (7 %), the emission intensity is weak because there are no sufficient luminescent centers. Higher than this value, the luminescent intensity decreases due to the concentration quenching effect based on the energy transfer between adjacent luminescent centers. Namely, the optimum concentration for red emission of Eu^{3+} is 7 % in YF_3:Eu^{3+} hollow nanofibers. Based on Dexter's theory [34], the average distances(R) between Eu^{3+} ions can be estimated by the following equation:

$$R = 2(3V/4\pi XN)^{1/3} \quad (1)$$

where V is the volume of the unit cell, X is the critical concentration, N is the number of available crystallographic sites occupied by the activator ions in the unit cell. For YF_3:Eu^{3+}, $V = 0.1914$ nm^3, $N = z \times 2 = 8$, and then the average distances(R) between Eu^{3+} ions is 0.8675 nm when the doping concentration is 7 %.

The fluorescent decay curves of YF_3:x%Eu^{3+} hollow nanofibers with different concentration of Eu^{3+} (1, 3, 5, 7,

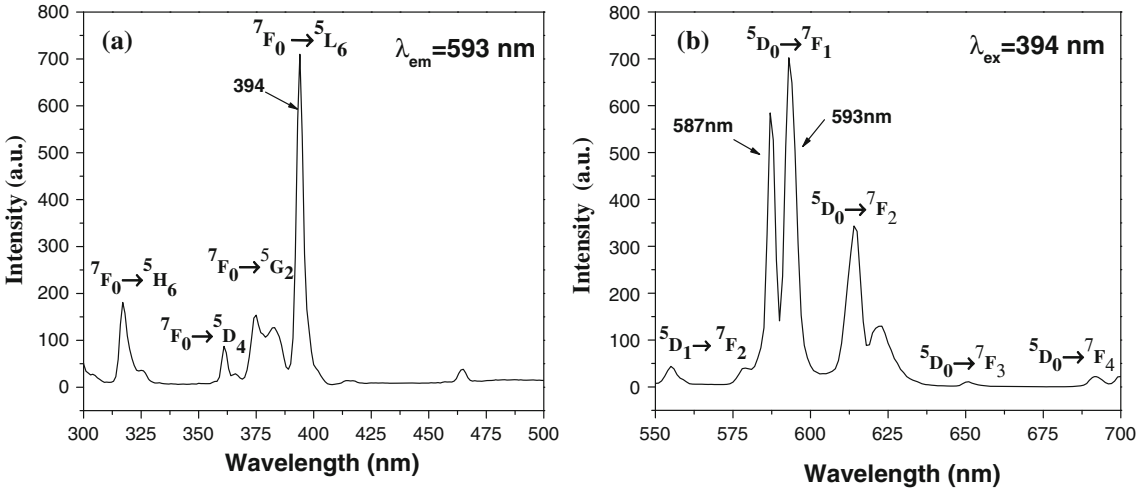

Fig. 7 Excitation spectrum (**a**) and emission spectrum (**b**) of YF_3:7%Eu^{3+} *hollow* nanofibers

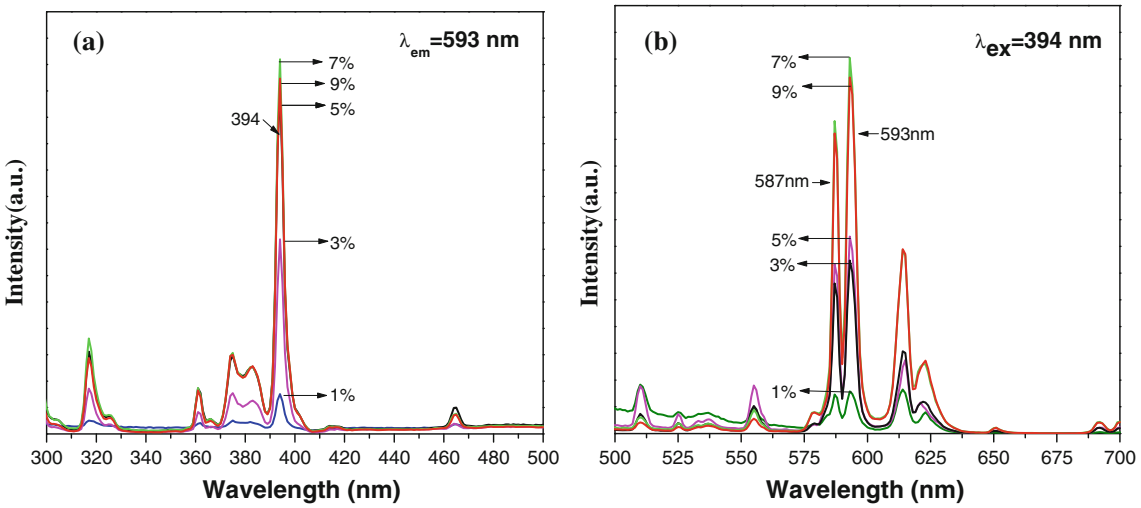

Fig. 8 Excitation (**a**) and emission (**b**) spectra of YF_3:*x*%Eu^{3+} (x = 1,3,5,7,9) *hollow* nanofibers

and 9 %), as presented in Fig. 9, are used to calculate the lifetime and to investigate the luminescence dynamics of these samples. The samples are excited by 394 nm and monitored by 593 nm, and the curves accord with the single exponential decay:

$$I_t = I_0 \exp(-t/\tau) \quad (2)$$

where I_t is the intensity at time t, I_0 is the intensity at $t = 0$ and τ is the decay lifetime [35]. All the curves can be fitted by single exponential procedures, and the lifetime values of YF_3:Eu^{3+} are 8.174, 11.916, 6.8818, 7.7203, and 7.1565 ms corresponding to the Eu^{3+} concentration of 1, 3, 5, 7, and 9 %, respectively.

In general, color can be represented by the Commission International del'Eclairage (CIE) 1931 chromaticity coordinates. The color coordinates for the red emission in the present experiment are calculated based on the corresponding emission spectra and the results are shown in Fig. 10. The

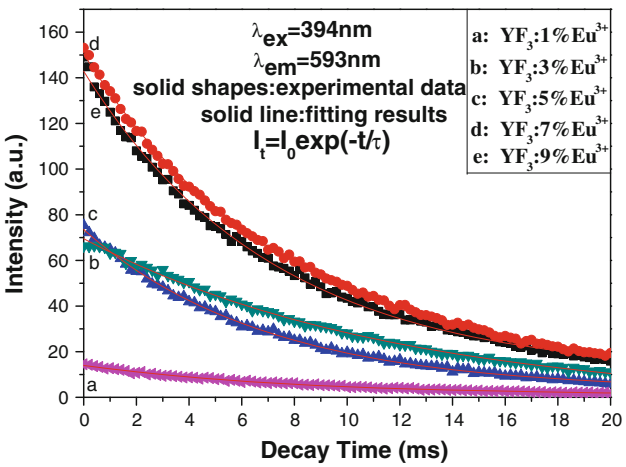

Fig. 9 Decay curves of YF_3:*x*%Eu^{3+} (x = 1,3,5,7,9) *hollow* nanofibers

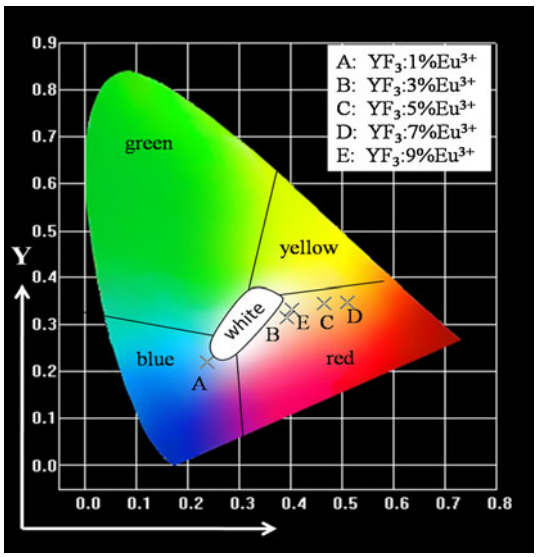

Fig. 10 CIE chromaticity coordinates diagram of YF_3:x%Eu^{3+} (x = 1,3,5,7,9) *hollow* nanofibers

coordinates (x, y) of YF_3:Eu^{3+} hollow nanofibers are (0.238, 0.220), (0.393, 0.315), (0.466, 0.344), (0.510, 0.348), and (0.402, 0.333) which correspond to the Eu^{3+} concentration of 1, 3, 5, 7, and 9 %, respectively. Among these hollow nanofibers, YF_3:1%Eu^{3+} hollow nanofibers show nearly blue emission owing to the presence of stronger intensity arising from $^5D_1 \rightarrow {}^7F_2$ transitions of Eu^{3+} ions. These results indicate that the emission colors of YF_3:Eu^{3+} hollow nanofibers are tunable by changing the concentration of doping Eu^{3+} ions, which is considered to be a promising candidate for application in LEDs [35].

Formation mechanism for YF_3:Eu^{3+} hollow nanofibers

We propose the formation mechanism for YF_3:Eu^{3+} hollow nanofibers, as shown in Fig. 11. First, the precursor

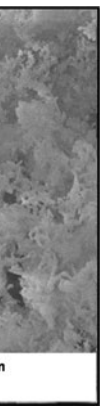

Fig. 12 SEM image of YF_3:Eu^{3+} particles prepared via direct mixing of Y_2O_3:Eu^{3+} *hollow* nanofibers with NH_4HF_2 powders

spinning solutions were prepared and PVP@PVP/[$Y(NO_3)_3$ + $Eu(NO_3)_3$] core–sheath composite nanofibers were fabricated by coaxial electrospinning, and then Y_2O_3:Eu^{3+} hollow nanofibers were prepared through calcining the as-obtained composite nanofibers. During calcination process, PVP chain was broken and volatilize. With the increase in calcination temperature, nitrate was decomposed and oxidized to NO_2, Y^{3+} and Eu^{3+} were oxidized to form Y_2O_3:Eu^{3+} crystallites, many crystallites were combined into nanoparticles, then some nanoparticles were mutually connected to generate hollow-centered Y_2O_3:Eu^{3+} nanofibers. Next, Y_2O_3:Eu^{3+} hollow nanofibers were fluorinated using NH_4HF_2 as fluorinating agent. In the fluorinated process, NH_4HF_2 decomposed and reacted with Y_2O_3:Eu^{3+} hollow nanofibers to produce YF_3:Eu^{3+} hollow nanofibers. During the process, NH_4HF_2 powders and Y_2O_3:Eu^{3+} hollow nanofibers were separated by the small crucible, which prevented Y_2O_3:Eu^{3+} hollow nanofibers from morphology damage. If Y_2O_3:Eu^{3+} hollow nanofibers directly mix with NH_4HF_2 powders, melted NH_4HF_2 will

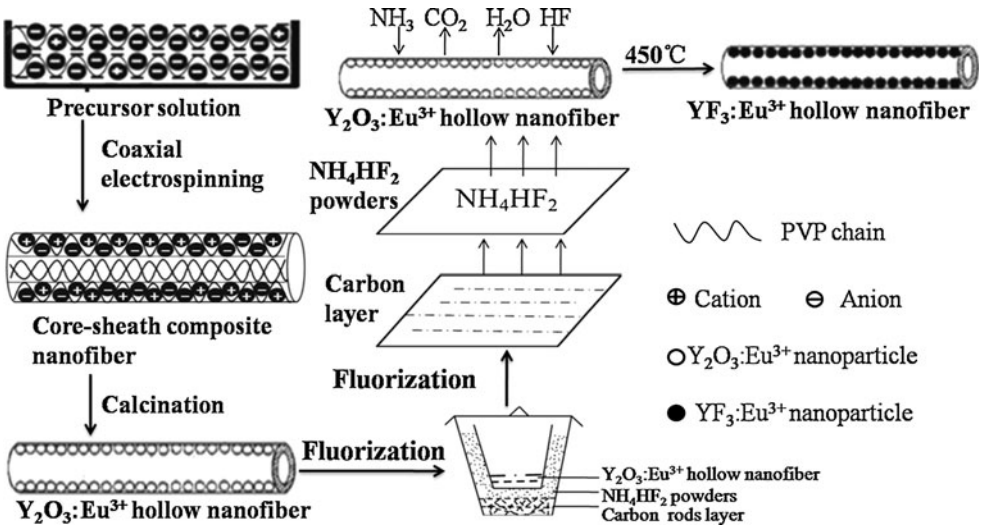

Fig. 11 Formation mechanism of YF_3:Eu^{3+} *hollow* nanofibers

cut the Y_2O_3:Eu^{3+} hollow nanofibers into pieces, as a result, the morphology of Y_2O_3:Eu^{3+} hollow nanofibers cannot be retained, as presented in Fig. 12. Carbon rods played an important role in the reduction via combination of O_2 to produced CO, which react with oxygen species of Y_2O_3:Eu^{3+} to give CO_2 in the heating process. The double-crucible method we proposed here is actually a solid–gas reaction, which has been proved to be an important method, not only can retain the morphology of Y_2O_3:Eu^{3+} hollow nanofibers, but also can fabricate YF_3:Eu^{3+} hollow nanofibers with pure phase at relatively low temperature.

Conclusions

In summary, orthorhombic structure YF_3:Eu^{3+} hollow nanofibers were successfully fabricated via fluorination of the relevant Y_2O_3:Eu^{3+} hollow nanofibers which were obtained by calcining the coaxial electrospun core–sheath composite nanofibers. The morphology of YF_3:Eu^{3+} hollow nanofibers can be inherited from Y_2O_3:Eu^{3+} hollow nanofibers under the fluorination circumstance via a double-crucible method we newly proposed. The mean diameter of YF_3:Eu^{3+} hollow nanofibers is 211 ± 29 nm. YF_3:Eu^{3+} hollow nanofibers emit red emissions of predominant peaks at 593 and 587 nm originating from $^5D_0 \rightarrow {}^7F_1$ transition of Eu^{3+} ions under the excitation of 394 nm ultraviolet light and the quenching concentration is 7 %. The present work provides a new route to fabricate hollow nanofibers of rare earth trifluoride.

Acknowledgements This study was financially supported by the National Natural Science Foundation of China (NSFC 50972020, 51072026), Ph.D. Programs Foundation of the Ministry of Education of China (20102216110002, 20112216120003), the Science and Technology Development Planning Project of Jilin Province (Grant Nos. 20070402, 20060504), and the Key Research Project of Science and Technology of Ministry of Education of China (Grant No. 207026).

References

1. Tian Y, Chen BJ, Li XP, Zhang JS, Tian BN, Sun JS, Cheng LH, Zhong HY, Zhong H, Hua RN (2012) J Solid State Chem 196:187
2. Zhong SL, Lu YH, Huang ZZ, Wang SP, Chen JJ (2010) Opt Mater 32:966
3. Zhu GX, Li YD, Lian HZ, Chen YZ, Liu SG (2010) Chin Chem Lett 21:624
4. Zhong SL, Wang SJ, Xu HL, Li CG, Huang YX, Wang SP, Xu R (2009) Mater Lett 63:530
5. Zhong HX, Hong JM, Cao XF, Chen XT, Xue ZL (2009) Mater Res Bull 44:623
6. Zhang DS, Qin WP, Wang GF, Wang LL, Zhu PF, Kim R, Ding FH, Zheng KZ, Liu N (2010) J Nanosci Nanotechnol 10:2032
7. Wang GF, Qin WP, Wei GD, Wang LL, Zhu PF, Kim R, Zhang DS, Ding FH, Zheng KZ (2009) J Fluor Chem 130:158
8. Wang GF, Qin WP, Zhang JS, Zhang JS, Wang Y, Cao CY, Wang LL, Wei GD, Zhu PF, Kim R (2008) J Fluor Chem 129:621
9. Zhu L, Cap X, Yang D (2011) Adv Mater Res 233–235:54
10. Zhang JS, Qin WP, Zhang JS, Wan Y, Cao CY, Jin Y, Wei GD, Wang GF, Wang LL (2007) Chem Res Chin 23:733
11. Guo FQ, Li HF, Zhang ZF, Meng SL, Li DQ (2009) Mater Sci Eng B 163:134
12. Xu ZH, Li CX, Yang PP, Zhang CM, Huang SS, Lin J (2009) Cryst Growth Des 9:4752
13. Wang SJ, Xu HL, Chen XS, Zhong SL, Jiang JW, Huang YX, Wang SP, Xu R (2008) J Cryst Growth 310:4697
14. Ma M, Xu CF, Yang LW, Ren GZ, Lin JG, Yang QB (2011) Phys B 406:3256
15. Li ZH, Zheng LZ, Zhang LN, Xiong LY (2007) J Lumin 126:481
16. Fujihara S, Koji S, Kadota Y, Kimura T (2004) J Am Ceram Soc 87:1659
17. Beauzamy L, Moine B, Gredin P (2007) J Lumin 127:568
18. Ni YH, Li GY, Hong JM (2010) Ultrason Sonochem 17:509
19. Guo FQ, Li HF, Zhang ZF, Meng SL, Li DQ (2009) Mater Res Bull 44:1565
20. Li GH, Lai YW, Bao WW, Li LL, Li MM, Gan SC (2011) Powder Technol 214:211
21. Zhang J, Choi SW, Kim SS (2011) J Solid State Chem 184:3008
22. Yang RY, Qin GS, Zhao D, Zheng KZ, Qin WP (2012) J Fluor Chem 140:38
23. Wei SH, Zhou MH, Du WP (2011) Sens Actuators B Chem 160:753
24. Wang JX, Dong XT, Cui QZ, Liu GX, Yu WS (2011) J Nanosci Nanotechnol 11:2514
25. Dong XT, Lui L, Wang JX, Liu GX (2010) Chem J Chin Univ 31:20
26. Cui QZ, Dong XT, Wang JX, Li M (2008) J Rare Earths 26:664
27. Ma QL, Wang JX, Dong XT, Yu WS, Liu GX, Xu J (2012) J Mater Chem 22:14438
28. Liu Y, Wang JX, Dong XT, Liu GX (2010) Chem J Chin Univ 31:1291
29. Yang LY, Wang JX, Dong XT, Liu GX, Yu WS (2013) J Mater Sci 48:644. doi:10.1007/s10853-012-6768-5
30. Zhang X, Shao CL, Zhang ZY, Li JH, Zhang P, Zhang MY, Mu JB, Guo ZC, Liang PP, Liu YC (2012) ASC Appl Mater Interfaces 4:785
31. Ma WW, Dong XT, Wang JX, Yu WS, Liu GX (2013) J Mater Sci 48:2557. doi:10.1007/s10853-012-7046-2
32. Yun KS, Byung WA, Kang TJ (2012) J Magn Magn Mater 324:916
33. Zhang H, Li HF, Li DQ, Meng SL (2006) J Colloid Interface Sci 302:509
34. Blasse G (1968) Phys Lett 28:444
35. Zhu ZF, Liu DG, Liu H, Li GJ, Du J, He ZL (2012) J Lumin 132:261